Zhigen Wu[1]
School of Civil Engineering,
Hefei University of Technology,
Hefei, Anhui 230009, China
e-mail: zhigenwu@hfut.edu.cn

Jixiang Meng
School of Civil Engineering,
Hefei University of Technology,
Hefei, Anhui 230009, China

Yihua Liu
School of Civil Engineering,
Hefei University of Technology,
Hefei, Anhui 230009, China

Hao Li
School of Civil Engineering,
Hefei University of Technology,
Hefei, Anhui 230009, China

Rui Huang[1]
Department of Aerospace Engineering
and Engineering Mechanics,
University of Texas,
Austin, TX 78712
e-mail: ruihuang@mail.utexas.edu

A State Space Method for Surface Instability of Elastic Layers With Material Properties Varying in Thickness Direction

*A state space method is proposed for analyzing surface instability of elastic layers with elastic properties varying in the thickness direction. By assuming linear elasticity with nonlinear kinematics, the governing equations for the incremental stress field from a fundamental state are derived for arbitrarily graded elastic layers subject to plane-strain compression, which lead to an eigenvalue problem. By discretizing the elastic properties into piecewise constant functions with homogeneous sublayers, a state space method is developed to solve the eigenvalue problem and predict the critical condition for onset of surface instability. Results are presented for homogeneous layers, bilayers, and continuously graded elastic layers. The state space solutions for elastic bilayers are in close agreement with the analytical solution for thin film wrinkling within the limit of linear elasticity. Numerical solutions for continuously graded elastic layers are compared to finite element results in a previous study (Lee et al., 2008, J. Mech. Phys. Solids, **56**, pp. 858–868). As a semi-analytical approach, the state space method is computationally efficient for graded elastic layers, especially for laminated multilayers.*
[DOI: 10.1115/1.4027464]

Keywords: state space method, surface instability, graded material, layered material

1 Introduction

Surface patterns are commonly observed in nature [1] and experiments [2–4]. A large number of these patterns result from surface instability. Extensive theoretical studies on surface instability have been devoted to two types: one is for a homogeneous block of a rubberlike elastic material when compressed beyond a moderately large strain [5,6], and the other is for a stiff skin layer on a soft substrate under compression [7–9]. Correspondingly, two types of surface instability patterns have been predicted, creases and wrinkles. Both creases and wrinkles set in by deviating from a state of homogenous deformation. Wrinkles deviate from the homogenous state by a field of infinitesimal strain in finite space, whereas creases deviate by a field of finite strain localized in space. In the case of a homogeneous elastic block, onset of creasing instability precedes that of wrinkling [10–12], with a critical strain in the regime of nonlinear elasticity. For a stiff skin layer on a soft substrate, the critical strain for wrinkling can be much smaller, typically within the limit of linear elasticity (i.e., less than a few percent). By changing the elastic modulus ratio in the bilayer system, a transition from wrinkling to creasing was predicted by Wang and Zhao [13]. More generally, an elastic layer could be functionally graded or laminated in multilayers with the elastic properties varying in the thickness direction, either continuously or discontinuously. Examples include human skins, poly(methyldisiloxane) with oxidized surface, and hydrogels with depthwise cross-link gradients. A few recent studies have considered surface instability of graded elastic layers. Lee et al. [14] presented a general bifurcation analysis for surface instability of an elastic half space with material properties varying in the thickness direction. Cao et al. [15] derived the critical condition for wrinkling of a stiff thin layer on a semi-infinite substrate with continuously graded elastic modulus. More recently, Diab et al. [16] presented a nonlinear bifurcation analysis for a neo-Hookean half space with its elastic properties decaying exponentially in depth. As noted by Lee et al. [14], except for a few special cases, the critical condition for onset of surface instability has to be determined numerically, and they used a finite element method to solve the eigenvalue problem for onset of surface wrinkling. In the present study, we propose an alternative, semi-analytical method by the concept of state space for generally graded or layered materials and show that the state space method is computationally efficient for the analysis of surface instability.

The remainder of this paper is organized as follows. Section 2 derives the governing equations for the incremental stress field in an orthotropic elastic layer with arbitrarily graded elastic properties. The state space method is presented in Sec. 3 to solve the eigenvalue problem for the critical condition of surface instability. The results are presented in Sec. 4, verifying the state space solution by comparing to the analytical solutions for elastic bilayers and the finite element results for continuously graded elastic layers. Section 5 concludes the present study with a short summary.

2 Theory of Elastic Surface Instability

Consider an elastic layer with one face being traction free and the other face attached to a rigid support as shown in Fig. 1(*a*), where a Cartesian coordinate system is set up such that $X_2 = 0$ at

[1]Corresponding authors.

Manuscript received March 24, 2014; final manuscript received April 17, 2014; accepted manuscript posted April 22, 2014; published online May 5, 2014. Editor: Yonggang Huang.

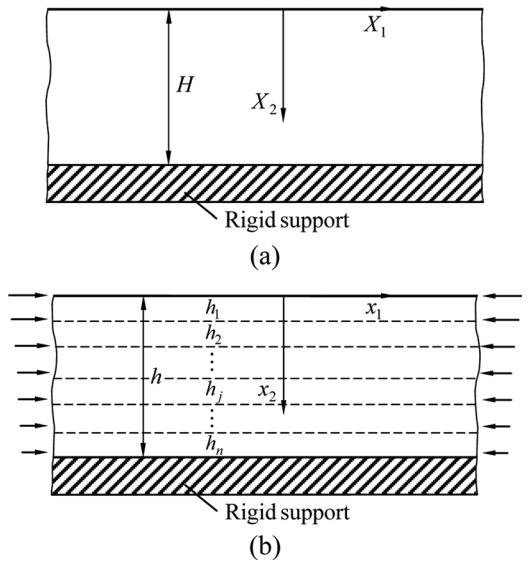

Fig. 1 Schematics of an elastic layer on a rigid support: (*a*) in the stress-free reference state and (*b*) in the fundamental state subjected to in-plane compression, divided into *n* sublayers for the state space method

the free surface and $X_2 = H$ at the interface between the layer and the support. When the elastic layer is subjected to an in-plane compression parallel to the free surface, the compressive stress inside the layer may cause surface instability. We refer to the compressed state with a flat surface as the fundamental state (Fig. 1(*b*)) and denote the corresponding coordinates as (x_1, x_2). In the present study, we focus on plane-strain compression with a uniform nominal strain in the x_1-direction, although the analysis can be readily extended to consider biaxial in-plane compression.

The material is assumed to be linear elastic with a quadratic strain energy density function in terms of Green–Lagrange strain

$$W = \frac{1}{2} C_{IJKL} E_{IJ} E_{KL} \tag{1}$$

where $E_{IJ} = \frac{1}{2}(F_{kI}F_{kJ} - \delta_{IJ})$, $F_{kJ} = \partial x_k / \partial X_J$, δ_{IJ} is the Kronecker delta, and C_{IJKL} is the elastic modulus. To facilitate a consistent stability analysis, it is necessary to consider nonlinear kinematics even for small deformation of constitutively linear elastic materials [14]. For an orthotropic elastic layer with material properties varying in the thickness direction, C_{IJKL} is a function of X_2 and possesses the orthotropic symmetry with respect to three orthogonal axes coinciding with the Cartesian coordinates.

With the strain energy density function, the second Piola–Kirchhoff stress is obtained as

$$S_{IJ} = \frac{\partial W}{\partial E_{IJ}} = C_{IJKL} E_{KL} \tag{2}$$

and the first Piola–Kirchhoff stress (nominal stress) is

$$P_{iJ} = \frac{\partial W}{\partial F_{iJ}} = F_{iK} S_{KJ} \tag{3}$$

The equilibrium equation can be written as

$$P_{iJ,J} = F_{iK} S_{KJ,J} + S_{KJ} F_{iK,J} = 0 \tag{4}$$

and the boundary condition at the free surface requires that

$$P_{i2} = 0, \quad \text{at} \quad X_2 = 0 \tag{5}$$

Here and subsequently, the notation $()_{,J}$ denotes differentiation with respect to X_J in the reference state, whereas $()_{,j}$ denotes differentiation with respect to x_j in the fundamental state; the Einstein summation convention is implied over repeated indices unless noted otherwise.

Under the plane-strain condition, the strain and stress in the fundamental state can be determined in terms of the imposed nominal strain, $\varepsilon_0 = F_{11} - 1$. The corresponding Green–Lagrange strain is: $E_{11} = \varepsilon_0 + (1/2)\varepsilon_0^2$. Strain compatibility requires that E_{11} be independent of X_2. The equilibrium equation and boundary conditions together require that $S_{22} = P_{22} = 0$ everywhere in the fundamental state, and hence

$$E_{22} = -\frac{C_{2211}}{C_{2222}}\left(\varepsilon_0 + \frac{1}{2}\varepsilon_0^2\right) \tag{6}$$

The compressive stress in the fundamental state is then

$$S_{11} = \left(C_{1111} - \frac{C_{1122}^2}{C_{2222}}\right)\left(\varepsilon_0 + \frac{1}{2}\varepsilon_0^2\right) \tag{7}$$

and $P_{11} = (1 + \varepsilon_0)S_{11}$. For the elastic layer with material properties varying in the thickness direction, both the lateral strain E_{22} and the compressive stress (S_{11} or P_{11}) vary with X_2 in general, hence inhomogeneous for the fundamental state.

Next consider an incremental displacements Δu_i $(i = 1, 2)$ from the fundamental state. The increments of the deformation gradient and the Green–Lagrange strain are

$$\Delta F_{kJ} = F_{iJ} \Delta u_{k,i} \tag{8}$$

$$\Delta E_{IJ} = \frac{1}{2}(F_{kI}F_{iJ} + F_{iI}F_{kJ})\Delta u_{k,i} \tag{9}$$

and correspondingly, the increments of the Piola–Kirchhoff stresses are

$$\Delta S_{IJ} = C_{IJKL} \Delta E_{KL} \tag{10}$$

$$\Delta P_{iJ} = F_{iK} \Delta S_{KJ} + S_{KJ} \Delta F_{iK} \tag{11}$$

The incremental stress field must satisfy the equilibrium equation and the boundary condition, i.e.,

$$\Delta P_{iJ,J} = (F_{iK} \Delta S_{KJ} + S_{KJ} \Delta F_{iK})_{,J} = 0 \tag{12}$$

$$\Delta P_{i2} = F_{iK} \Delta S_{K2} + S_{K2} \Delta F_{iK} = 0, \quad \text{at} \quad X_2 = 0 \tag{13}$$

Assuming that the strain in the fundamental state is small so that $F_{iK} \approx \delta_{iK}$, the increment of the first Piola–Kirchhoff stress in Eq. (11) can be approximated as

$$\Delta P_{iJ} \approx C_{iJkl} \Delta u_{k,l} + P_{kJ} \Delta u_{i,k} \tag{14}$$

Inserting Eq. (14) into Eqs. (12) and (13), the equilibrium equation and boundary condition become

$$(C_{iJkl} \Delta u_{k,l} + P_{kJ} \Delta u_{i,k})_{,J} = 0 \tag{15}$$

$$C_{i2kl} \Delta u_{k,l} + P_{k2} \Delta u_{i,k} = 0, \quad \text{at} \quad x_2 = 0 \tag{16}$$

Equations (15) and (16) are essentially identical to Eqs. (10) and (11) in Ref. [14], which were derived from a variational approach under the same assumptions of linear elasticity and small strain.

However, it is noted that the stress in the fundamental state given by Eq. (1) in Ref. [14] is incorrect, but their numerical results seem to be unaffected.

In addition, attachment to the rigid support imposes a boundary condition for the incremental displacement at the bottom of the elastic layer

$$\Delta u_i = 0, \quad \text{at} \quad x_2 = h \tag{17}$$

The equilibrium equation (15) along with the boundary conditions (16) and (17) constitutes an eigenvalue problem. The fundamental state becomes unstable when there exist any nontrivial solutions for the incremental field, and surface instability is expected for the specific boundary conditions. The critical condition for onset of surface instability is predicted by solving the eigenvalue problem. However, for an arbitrarily graded elastic layer with $C_{ijkl}(x_2)$, the problem in the general case cannot be solved analytically. Lee et al. [14] developed a finite element method by discretizing the governing equations. Their numerical results for elastic bilayers agree well with the analytical solution for wrinkling of thin films by Huang et al. [8], but for continuously graded elastic layers the numerical results were not benchmarked since no analytical solutions were available. In the present study we develop a state space method to solve the eigenvalue problem for arbitrarily graded elastic layers (including multilayers). We note that the present study is limited by the assumptions of linear elasticity and small strain. This limitation may be removed by using a strain energy density function of nonlinear elasticity in a generally finite-strain formulation, as shown for hydrogel layers in a previous study [17].

3 State Space Method

In this section, we first present the state equation for a homogeneous layer and then use this equation to analyze surface instability of elastic layers with graded material properties. The state space method is commonly used in dynamic systems to analyze multiple inputs and outputs related by differential equations (also known as the "time-domain approach") [18,19].

3.1 State Equation for a Homogeneous Layer. Assuming the elastic layer is homogeneous and isotropic, the incremental stress in Eq. (14) becomes

$$\Delta P_{11} = (\lambda + 2\mu + P_{11})\Delta u_{1,1} + \lambda \Delta u_{2,2} \tag{18}$$

$$\Delta P_{12} = \mu(\Delta u_{1,2} + \Delta u_{2,1}) \tag{19}$$

$$\Delta P_{21} = \mu \Delta u_{1,2} + (\mu + P_{11})\Delta u_{2,1} \tag{20}$$

$$\Delta P_{22} = \lambda \Delta u_{1,1} + (\lambda + 2\mu)\Delta u_{2,2} \tag{21}$$

where the fundamental nominal stress $P_{11} \approx (4\mu(\lambda + \mu)/(\lambda + 2\mu))\varepsilon_0$ with λ and μ being Lame's constants of isotropic elasticity. The incremental stress satisfies the equilibrium equations

$$\frac{\partial \Delta P_{11}}{\partial x_1} + \frac{\partial \Delta P_{12}}{\partial x_2} = 0 \tag{22}$$

$$\frac{\partial \Delta P_{21}}{\partial x_1} + \frac{\partial \Delta P_{22}}{\partial x_2} = 0 \tag{23}$$

and the boundary condition

$$\Delta P_{22} = \Delta P_{12} = 0, \quad \text{at} \quad x_2 = 0 \tag{24}$$

Let α denote the differentiation with respect to x_1. From Eqs. (19) and (21), we have

$$\Delta u_{1,2} = \frac{1}{\mu}\Delta P_{12} - \alpha \Delta u_2 \tag{25}$$

$$\Delta u_{2,2} = \frac{1}{\lambda + 2\mu}(\Delta P_{22} - \lambda \alpha \Delta u_1) \tag{26}$$

Differentiation of Eqs. (18) and (20) with respect to x_1 yields

$$\alpha \Delta P_{11} = (\lambda + 2\mu + P_{11})\alpha^2 \Delta u_1 + \lambda \alpha \Delta u_{2,2} \tag{27}$$

$$\alpha \Delta P_{21} = \mu \alpha \Delta u_{1,2} + (\mu + P_{11})\alpha^2 \Delta u_2 \tag{28}$$

Substituting Eqs. (25) and (26) into Eqs. (27) and (28) and then into Eqs. (22) and (23), we obtain that

$$\Delta P_{12,2} = -\left[\frac{4\mu(\lambda + \mu)}{\lambda + 2\mu} + P_{11}\right]\alpha^2 \Delta u_1 - \frac{\lambda}{\lambda + 2\mu}\alpha \Delta P_{22} \tag{29}$$

$$\Delta P_{22,2} = -P_{11}\alpha^2 \Delta u_2 - \alpha \Delta P_{12} \tag{30}$$

Assume the perturbation displacements to be sinusoidal in the x_1 direction, namely

$$\Delta u_1 = U_1(x_2)\sin(\omega x_1) \quad \text{and} \quad \Delta u_2 = U_2(x_2)\cos(\omega x_1) \tag{31}$$

where ω is the wave number. Correspondingly, the incremental stresses are

$$\Delta P_{12} = T_1(x_2)\sin(\omega x_1) \quad \text{and} \quad \Delta P_{22} = T_2(x_2)\cos(\omega x_1) \tag{32}$$

Inserting Eqs. (31) and (32) into Eqs. (25), (26), (29), and (30), a set of differential equations are obtained in a matrix form as

$$\frac{\mathrm{d}}{\mathrm{d}x_2}\begin{Bmatrix} U_1(x_2) \\ T_2(x_2) \\ U_2(x_2) \\ T_1(x_2) \end{Bmatrix} = \mathbf{A}\begin{Bmatrix} U_1(x_2) \\ T_2(x_2) \\ U_2(x_2) \\ T_1(x_2) \end{Bmatrix} \tag{33}$$

where

$$\mathbf{A} = \begin{bmatrix} 0 & 0 & \omega & \dfrac{1}{\mu} \\ 0 & 0 & P_{11}\omega^2 & -\omega \\ -\dfrac{\lambda\omega}{\lambda + 2\mu} & \dfrac{1}{\lambda + 2\mu} & 0 & 0 \\ \left[\dfrac{4\mu(\lambda + \mu)}{\lambda + 2\mu} + P_{11}\right]\omega^2 & \dfrac{\lambda\omega}{\lambda + 2\mu} & 0 & 0 \end{bmatrix} \tag{34}$$

Equation (33) defines a set of first-order, homogeneous, ordinary differential equations in terms of the displacements and tractions, which is commonly called the state equation [20]. By integrating the differential equations, the state vector, $[U_1, T_2, U_2, T_1]$, can be determined as

$$\begin{Bmatrix} U_1(x_2) \\ T_2(x_2) \\ U_2(x_2) \\ T_1(x_2) \end{Bmatrix} = \mathbf{D}(x_2)\begin{Bmatrix} U_1(0) \\ T_2(0) \\ U_2(0) \\ T_1(0) \end{Bmatrix} = \mathrm{e}^{\mathbf{A}x_2}\begin{Bmatrix} U_1(0) \\ T_2(0) \\ U_2(0) \\ T_1(0) \end{Bmatrix} \tag{35}$$

where the state vector at x_2 is related to the same state vector at $x_2 = 0$. The matrix, $\mathbf{D}(x_2) = \mathrm{e}^{\mathbf{A}x_2}$, can be calculated directly by the matrix exponential operation (e.g., expm in Matlab), which maps one matrix ($\mathbf{A}$) to another ($\mathbf{D}$) as follows:

$$\mathbf{D}(x_2) = \mathrm{e}^{\mathbf{A}x_2} = \mathbf{V} \cdot \mathrm{e}^{\mathbf{\Lambda}x_2} \cdot \mathbf{V}^{-1} \tag{36}$$

where $\mathbf{\Lambda}$ is a diagonal matrix with the eigenvalues of the matrix $\mathbf{A}$ and $\mathbf{V}$ is the corresponding matrix with the eigenvectors so that

$\mathbf{A} = \mathbf{V} \cdot \mathbf{\Lambda} \cdot \mathbf{V}^{-1}$. Exponentiation of a diagonal matrix can be obtained simply by exponentiation of the diagonal elements.

The boundary conditions in Eqs. (17) and (24) dictate that

$$U_1(h) = U_2(h) = 0 \tag{37}$$

$$T_2(0) = T_1(0) = 0 \tag{38}$$

For a homogeneous elastic layer, substituting Eqs. (37) and (38) into Eq. (35), we obtain

$$\begin{Bmatrix} 0 \\ T_2(h) \\ 0 \\ T_1(h) \end{Bmatrix} = \mathbf{D}(h) \begin{Bmatrix} U_1(0) \\ 0 \\ U_2(0) \\ 0 \end{Bmatrix} \tag{39}$$

which leads to an eigenvalue problem in terms of the surface displacements

$$D_{11}U_1(0) + D_{13}U_2(0) = 0 \tag{40}$$

$$D_{31}U_1(0) + D_{33}U_2(0) = 0 \tag{41}$$

To have a nontrivial solution for the surface displacements, the determinant of the coefficient matrix in Eqs. (40) and (41) must vanish, namely

$$D_{11}D_{33} - D_{13}D_{31} = 0 \tag{42}$$

which predicts the critical condition for onset of surface instability of the elastic layer. By a dimensional consideration, the critical condition for a homogeneous layer can be written as

$$\varepsilon_c = f(\omega h, \nu) \tag{43}$$

where $\varepsilon_c = -((\lambda + 2\mu)/(4\mu(\lambda + \mu)))P_{11}^c$ defines a critical strain corresponding to the critical stress P_{11}^c and $\nu = \lambda/(2(\lambda + \mu))$ is Poisson's ratio.

An alternative method is presented in the Appendix, which yields an explicit equation for the critical strain (Eq. A10). However, the explicit result is limited to a homogeneous layer, while the state space method can be readily extended to multilayered or graded elastic layers (Sec. 3.2).

3.2 State Space Solution for Graded Layers. Next we consider an elastic layer with its elastic properties varying in the thickness direction, described by two functions, $\lambda(x_2)$ and $\mu(x_2)$. The functions may be continuous (such as functionally graded elastic layers) or discontinuous (such as piecewise constant functions for bilayers or multilayer laminates). In either case, we divide the elastic layer into a number of homogeneous sublayers (Fig. 1(*b*)). In the case of a continuously graded elastic layer, the functions $\lambda(x_2)$ and $\mu(x_2)$ are discretized into piecewise constant functions with n sublayers. When n approaches infinity and the thickness of each sublayer approaches zero, the discretization would eventually converge toward the continuous functions. In practice, the continuously graded elastic layer can be analyzed exactly by the discretized sublayers with a finite but sufficiently large n. Therefore, regardless of continuous or discontinuous variation in the elastic properties, surface instability of the elastic layer can be analyzed by solving the state equation for each homogeneous sublayer as presented in Sec. 3.1, with the following steps.

As shown in Fig. 1(*b*), for the jth sublayer with thickness h_j, the elastic properties are approximately taken as

$$\lambda_j = [\lambda(y_{j-1}) + \lambda(y_j)]/2 \quad \text{and} \quad \mu_j = [\mu(y_{j-1}) + \mu(y_j)]/2 \tag{44}$$

where $y_j = h_1 + h_2 + \cdots + h_j$ and $y_0 = 0$. From the state space solution in Eq. (35), the state vector at the interface $x_2 = y_j$ is related to that at $x_2 = y_{j-1}$ as

$$\mathbf{R}(y_j) = \mathbf{D}_j(h_j)\mathbf{R}(y_{j-1}) \tag{45}$$

where $\mathbf{R}(y_j) = [U_1(y_j), T_2(y_j), U_2(y_j), T_1(y_j)]^T$, $\mathbf{D}_j(h_j) = \exp(\mathbf{A}_j h_j)$ (no summation over j), and the matrix $\mathbf{A}_j$ is given by Eq. (34) for each sublayer.

Noting the continuity of the state vector (displacements and tractions) across all interfaces between the sublayers, we obtain the following relation:

$$\mathbf{R}(y_n) = \mathbf{K}\mathbf{R}(0) \tag{46}$$

where $\mathbf{K} = \prod_{j=n}^{1} \mathbf{D}_j(h_j)$, with $\mathbf{R}(0)$ and $\mathbf{R}(y_n)$ being the state vectors at the surface ($x_2 = 0$) and the bottom ($x_2 = y_n = h$) of the elastic layer, respectively. The boundary conditions in Eqs. (37) and (38) require that

$$U_1(y_n) = U_2(y_n) = 0 \tag{47}$$

$$T_2(0) = T_1(0) = 0 \tag{48}$$

Inserting Eqs. (47) and (48) into Eq. (46), we obtain

$$\begin{Bmatrix} 0 \\ T_2(y_n) \\ 0 \\ T_1(y_n) \end{Bmatrix} = \mathbf{K} \begin{Bmatrix} U_1(0) \\ 0 \\ U_2(0) \\ 0 \end{Bmatrix} \tag{49}$$

which leads to an eigenvalue problem in terms of the surface displacements

$$K_{11}U_1(0) + K_{13}U_2(0) = 0 \tag{50}$$

$$K_{31}U_1(0) + K_{33}U_2(0) = 0 \tag{51}$$

Similar to the case of a homogeneous layer, the critical condition for onset of surface instability of the laminated layer is determined by the existence of nontrivial solutions to Eqs. (50) and (51), which requires that

$$K_{11}K_{33} - K_{13}K_{31} = 0 \tag{52}$$

Equation (52) presents an implicit relation between the critical strain ε_c and the dimensionless wave number ωh, which depends on the discretized material properties (λ_j and μ_j) and thickness (h_j) of each sublayer. Note that the corresponding critical stress varies with the elastic modulus in the sublayers. By a dimensional consideration, the critical condition can be written as

$$\varepsilon_c = f_n(\omega h, E_j/E_1, \nu_j, h_j/h; j = 1 \ldots n) \tag{53}$$

where $E_j = (\mu_j(3\lambda_j + 2\mu_j)/(\lambda_j + \mu_j))$ is Young's modulus of the jth sublayer.

In practice, the state equation can be normalized for each sublayer to yield a dimensionless matrix $\mathbf{D}$, which helps preventing the matrix $\mathbf{K}$ from ill-conditioning after multiplication of a large number of $\mathbf{D}$-matrices. The present state space method is applicable under the condition of linear elasticity and small-strain approximations. While the present study assumes a flat surface before instability, the state space method in principle can be extended to analyze instability of curved surfaces, such as radially graded elastic cylinders [21], which is left for future studies.

4 Results and Discussion

In this section, we present results for homogeneous elastic layers, bilayers, and continuously graded elastic layers. A bilayer

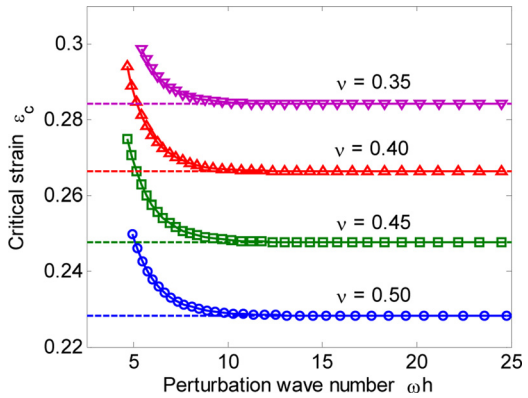

Fig. 2 The critical strain versus the perturbation wave number for homogeneous elastic layers with various Poisson's ratios. The horizontal dashed lines represent the analytical solutions for $\omega h \to \infty$, obtained from Eq. (A10).

with an elastic thin film on an elastic substrate is considered as a benchmark problem, for which the state space solution is compare to an analytical solution. For continuously graded elastic layers, the state space method offers an approximate solution by discretizing the elastic properties. Alternatively, Lee et al. [14] developed a finite element method by discretizing the differential equations. In both methods, the approximate solution converges when a sufficient number of discrete sublayers (or elements) are used.

4.1 Surface Instability of a Homogeneous Elastic Layer. For a homogeneous elastic layer, the critical condition for onset of surface stability can be obtained from Eq. (42) in terms of either a critical stress (P_{11}^c) or a critical strain (ε_c). Figure 2 plots the critical strain ε_c as a function of the perturbation wave number ωh. As the wave number increases, the critical strain decreases and approaches a constant as $\omega h \to \infty$. Thus, the critical condition for the surface instability of a homogeneous elastic layer is determined by the short-wave limit, independent of the layer thickness. This is similar to swell-induced surface instability of a hydrogel layer [22]. The critical strain at the short-wave limit for a homogeneous elastic layer can also be obtained analytically from Eq. (A10), shown as the horizontal dashed lines in Fig. 2. Evidently, the state space solution coincides with the analytical solution for $\omega h \to \infty$. The critical condition may be compared to Biot's analysis for an elastomer half space [5]. While Biot assumed a neo-Hookean nonlinear elasticity with a finite-strain formulation, the present study has assumed constitutively linear elasticity along with the small-strain approximation. As a result, the critical strain obtained from the present analysis is considerably lower than Biot's prediction ($\varepsilon_c = 0.46$). Apparently, the critical strain for a homogeneous elastic layer is beyond the small-strain approximation. Depending on the material, such a large strain could cause nonlinear elasticity, plasticity, or other types of instability (e.g., shear bands) before onset of the surface instability. In the case of an elastomer, it has been found that surface creasing precedes surface wrinkling as the primary mode of surface instability [10–12].

Most of the previous studies on surface instability of a homogeneous layer have assumed the material to be incompressible.

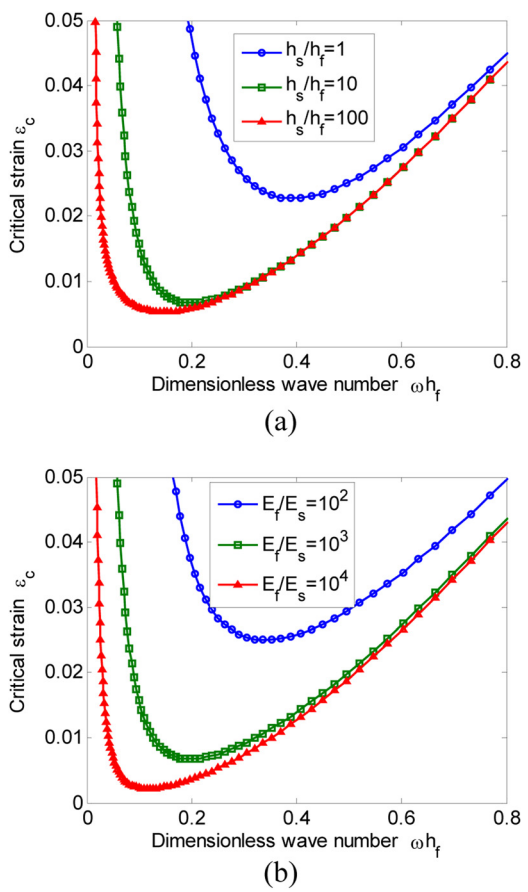

Fig. 3 The critical strain versus dimensionless wave number for elastic bilayers with $\nu_f = \nu_s = 0.4$: (*a*) $E_f/E_s = 1000$ and (*b*) $h_s/h_f = 10$

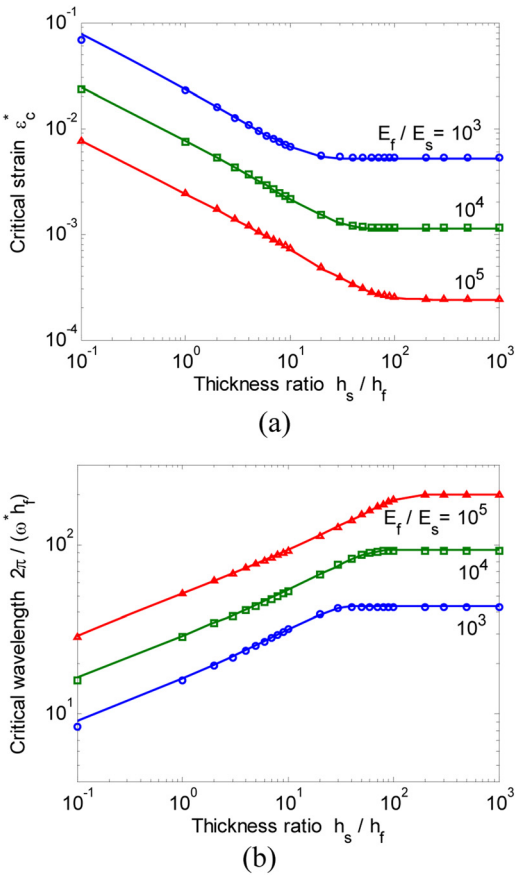

Fig. 4 (*a*) The critical strain for onset of surface instability and (*b*) the corresponding critical wavelength versus the thickness ratio for elastic bilayers with $\nu_f = \nu_s = 0.4$. The solid lines are predicted by the analytical solution [8].

Although quantitatively inaccurate, the present analysis predicts a qualitative trend that the critical strain depends on Poisson's ratio or in general the compressibility of the elastic material. As shown in Fig. 2, the critical strain increases as Poisson's ratio decreases (increasingly compressible).

4.2 Surface Instability of Elastic Bilayers. For an elastic bilayer, the critical condition for surface instability depends on the stiffness ratio between the two sublayers. When the surface layer is much stiffer than the underlayer, the critical strain is small and within the linear elasticity regime, as predicted analytically by Huang et al. [8] and many others [23–25]. Lee et al. [14] compared their numerical results to the analytical solution as a benchmark. Here we show that the state space solution for an elastic bilayer is in close agreement with the analytical solution. Following the notation in Ref. [14], let h_f and h_s be the thicknesses of the upper layer (film) and the underlayer (substrate), respectively, and $h = h_f + h_s$. Young's moduli for the two layers are E_f and E_s, and their Poisson's ratios are ν_f and ν_s.

For a bilayer, the matrix in Eq. (46) is simply $\mathbf{K} = \mathbf{D}_s(h_s)\,\mathbf{D}_f(h_f)$, where $\mathbf{D}_s(h_s)$ and $\mathbf{D}_f(h_f)$ are the matrix exponentials for the two homogeneous sublayers as defined in Eq. (36). By solving the eigenvalue problem in Eqs. (50) and (51), we obtain from Eq. (52) the critical strain ε_c as a function of the dimensionless wave number ωh_f, as shown in Fig. 3. For a fixed stiffness ratio (E_f/E_s), the critical strain decreases with increasing thickness ratio (h_s/h_f) as shown in Fig. 3(*a*). For a fixed thickness ratio, the critical strain decreases with increasing modulus ratio, as shown in Fig. 3(*b*). In all cases with $E_f/E_s > 1$, the critical strain is minimized at a finite wavenumber, defining a specific instability mode with wavenumber ω^* and the corresponding critical strain ε_c^*. The onset of surface instability is then predicted at the critical strain ε_c^*, with the corresponding wavelength $2\pi/\omega^*$.

The critical strain ε_c^* and the wavelength $2\pi/\omega^*$, normalized by the thickness of the upper layer (h_f), are plotted in Fig. 4 as functions of the thickness ratio h_s/h_f, in comparison with the analytical solution for thin film wrinkling [8]. The results from the state space method are found to be in excellent agreement with the analytical solution. We note that the finite element results by Lee et al. [14] were also in good agreement with the analytical solution. However, using the finite element method, 200 elements had to be used in order to achieve sufficient accuracy. In contrast, with two sublayers, the state space method requires only two four-by-four matrices and the solution is exact for the eigenvalue problem. In general, the state space method can be effectively extended for elastic layers with piecewise constant elastic properties (such as multilayers).

Both the minimum critical strain and the corresponding wavelength depend on the modulus ratio for elastic bilayers, as shown in Fig. 5. As the modulus ratio E_f/E_s decreases, the critical strain increases and the wavelength decreases. When the modulus ratio approaches one ($E_f/E_s \to 1$), the critical strain approaches that for a homogeneous layer, with $\varepsilon_c = 0.266$ for $\nu = 0.4$ as shown in Fig. 2. Interestingly, the corresponding wavelength in Fig. 5(*b*) approaches a finite value (~3.7), instead of zero wavelength

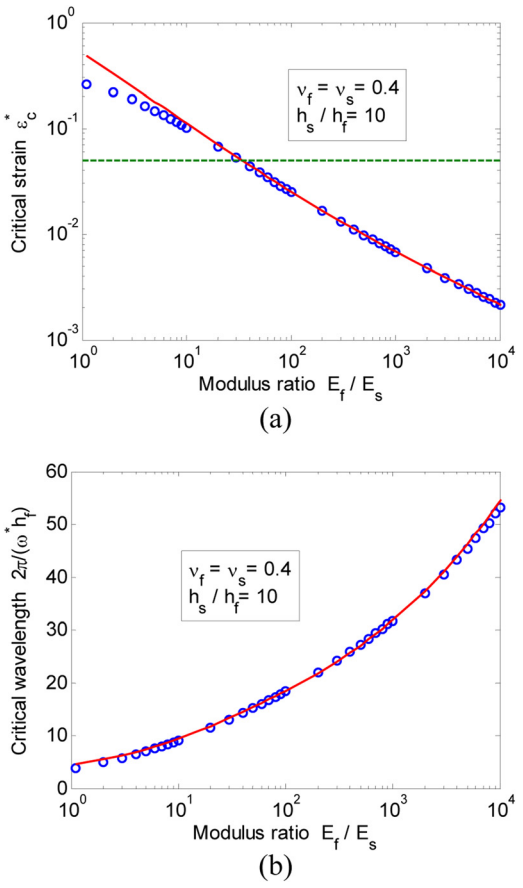

Fig. 5 (*a*) The critical strain for onset of surface instability and (*b*) the corresponding critical wavelength versus the modulus ratio for elastic bilayers. The solid lines are predicted by the analytical solution [8], and the horizontal dashed line in (*a*) suggests an upper bound for the small-strain approximation.

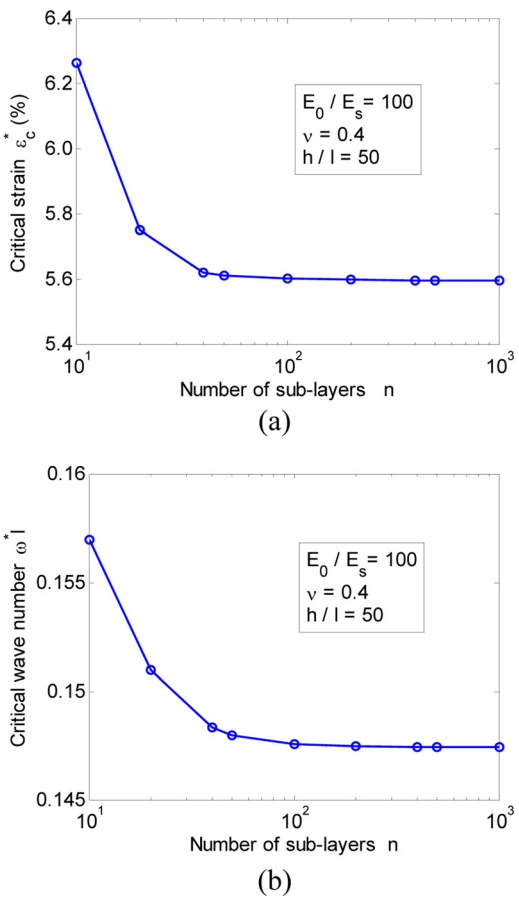

Fig. 6 Convergence of the state space solution for an exponentially graded elastic layer: (*a*) the critical strain and (*b*) the corresponding wave number, versus the number of sublayers used

expected for a homogeneous layer. This behavior is similar to a hydrogel bilayer considered in a previous study [17], where a metastable long-wavelength mode was predicted for modulus ratio less than 1. As the modulus ratio approaches 1 from either side, the long-wavelength mode persists while the corresponding critical strain approaches that for the zero-wavelength mode (short-wave limit), analogous to a first-order phase transition. As long as $E_f/E_s > 1$, the critical strain for the long-wave mode is lower than the short-wave limit for a homogeneous layer. Similar transition was considered by Wang and Zhao [13] based on energy minimization, but their numerical results predicted a critical modulus ratio greater than 1.

We note that the assumption of linear elasticity limits the present method to small strains. Taking $\varepsilon_c^* = 0.05$ as the upper bound for the assumption to be valid, the minimum modulus ratio in Fig. 5(*a*) is around 30, below which a nonlinear finite-strain formulation must be employed for more accurate analysis. The analytical solution by Huang et al. [8] is subject to the same limit of linear elasticity. In addition, the use of classical plate theory for the surface layer requires that the wavelength be much larger than the thickness ($2\pi/\omega^* \gg h_f$) in the analytical solution [25]; this limitation is removed in the state space solution. As shown in Fig. 5, when the stiffness ratio E_f/E_s is relatively large, the normalized critical wavelength is long and the critical strain predicted by the analytical solution agrees closely with the state space solution. However, as the stiffness ratio decreases, the critical wavelength decreases and the analytical solution becomes less accurate in comparison with the state space solution. However, within the limit of linear elasticity ($\varepsilon_c^* < 0.05$), the two solutions are nearly indistinguishable.

4.3 Elastic Layers With Continuously Graded Modulus. Following Lee et al. [14], we consider two types of elastic layers with the plane-strain modulus varying in the thickness direction as an exponential function and a complementary error function, respectively

$$\bar{E}(x_2) = \bar{E}_s + (\bar{E}_0 - \bar{E}_s)\exp\left(\frac{-x_2}{l}\right) \tag{54}$$

$$\bar{E}(x_2) = \bar{E}_s + (\bar{E}_0 - \bar{E}_s)\mathrm{erfc}\left(\frac{x_2}{l}\right) \tag{55}$$

where $\bar{E}_0$ and $\bar{E}_s$ refer to the plane-strain moduli at the surface ($x_2 = 0$) and the bottom ($x_2 = h \to \infty$) of the graded elastic layer, and the parameter l is a characteristic length for the modulus gradient. Poisson's ratio is taken to be a constant $\nu = 0.4$ in both cases.

For the continuously graded elastic layers, the elastic properties are discretized by dividing the layer into many homogeneous sublayers. A sufficiently large number of sublayers should be used in the state space method to ensure the accuracy of the results, similar to the convergence requirement for the finite element method. For an exponentially graded elastic layer with $\bar{E}_0/\bar{E}_s = 100$ and $h/l = 50$, by Eq. (54), $\bar{E}(x_2)$ is essentially equal to $\bar{E}_s$ for $x_2 \geq 20l$. Thus, the layer can be divided into $n-1$ uniform

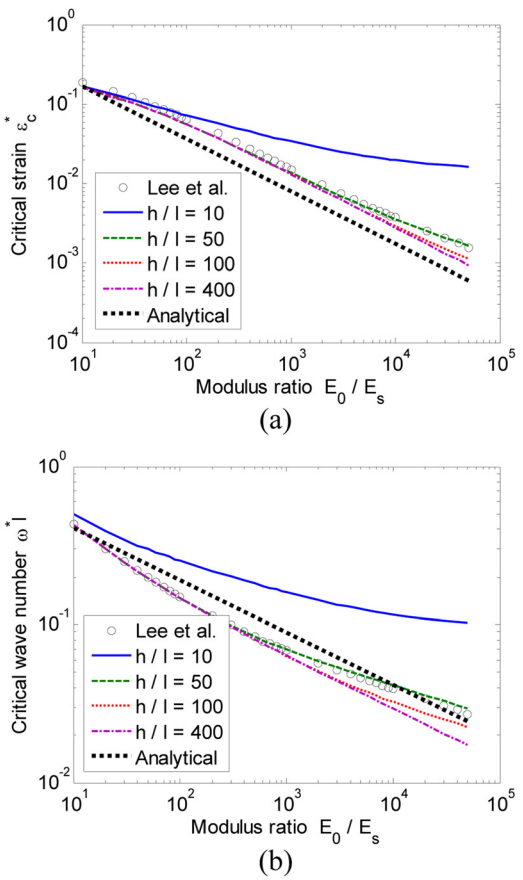

Fig. 7 (*a*) The critical strain and (*b*) the corresponding wave number for exponentially graded elastic layers with $\bar{E}_0/\bar{E}_s$ ranging from 10 to 10^5, comparing the state space solutions with the finite element results by Lee et al. [14] and the analytical approximation

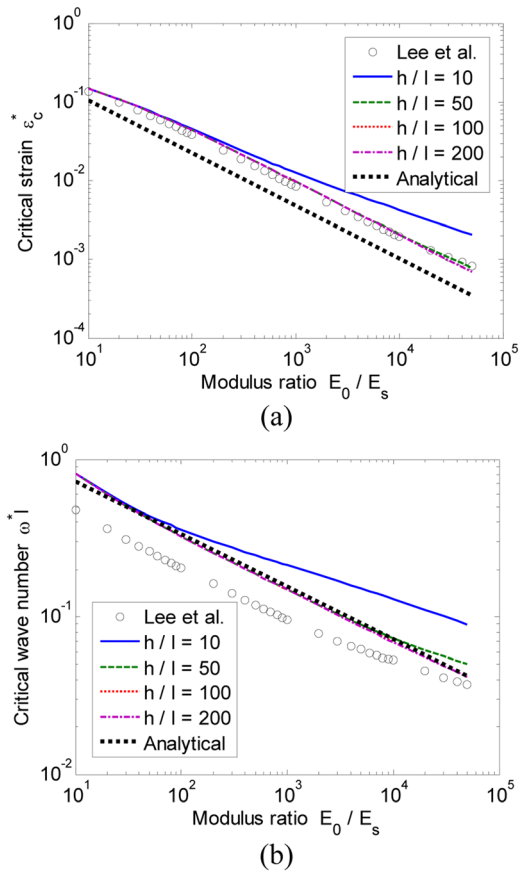

Fig. 8 (*a*) The critical strain and (*b*) the corresponding wave number, for the graded elastic layers with an error function for the plane-strain modulus, comparing the state space solutions with the finite element results by Lee et al. [14] and the analytical approximation

sublayers for $0 \le x_2 < 20l$ and one sublayer for $x_2 \ge 20l$ (almost homogeneous). Similar to the bilayer case, a minimum critical strain ε_c^* is predicted at a specific wavenumber, ω^*. Figure 6 shows the convergence of the state space solution with respect to the number of sublayers. It is observed that both ε_c^* and $\omega^* l$ decrease monotonically with the increasing number of sublayers, eventually converging toward the values of 0.0560 and 0.1474, respectively, for $n \ge 200$. Similar number of elements would have to be used to achieve convergence by the finite element method although the exact number was not given in Ref. [14].

Figure 7 shows the critical strain ε_c^* and the corresponding dimensionless wave number $\omega^* l$ as the modulus ratio $(\bar{E}_0/\bar{E}_s)$ changes from 10 to 10^5. Both the critical strain and the critical wave number decrease monotonically with the increasing modulus ratio, similar to Fig. 5 for the elastic bilayers. In addition, when the relative thickness h/l increases, both ε_c^* and $\omega^* l$ show converging trends, similar to Fig. 4 for the bilayers with the increasing thickness ratio. Interestingly, we notice that the results for $h/l = 50$ agree well with the finite element results in Ref. [14], which differ slightly from the limiting case with $h/l \to \infty$, i.e., a half space. An "equivalent homogeneous layer" was suggested by Lee et al. [14] as an approximation for the continuously graded elastic layer, with which an analytical solution can be obtained based on the bilayer model. As shown in Fig. 7, the analytical approximation underestimates the critical strain and overestimates the wavenumber, in comparison with the state space solutions for $h/l > 100$.

The critical strain ε_c^* and the corresponding dimensionless wave number $\omega^* l$ for the graded elastic layers described by the error function in Eq. (55) are shown in Fig. 8 with the modulus ratio $(\bar{E}_0/\bar{E}_s)$ varying from 10 to 10^5. Similar to Fig. 7, ε_c^* and $\omega^* l$ have the same trends with the increasing $\bar{E}_0/\bar{E}_s$ and h/l. We find that the results for $h/l = 100$ and 200 are nearly indistinguishable, suggesting that both ε_c^* and $\omega^* l$ for the error function grading converge faster with increasing h/l than for the exponential function. The faster convergence rate may be attributed to the fact that the error function decays more rapidly than the exponential function. For $h/l = 50$, the critical strain ε_c^* is again in good agreement with the finite element results [14], but the corresponding wave number $\omega^* l$ is considerably greater than the previous numerical results. Interestingly, the analytical approximation by the "equivalent homogeneous layer" compares closely with the predicted wavenumber by the state space solution for $h/l > 100$ in Fig. 8(*b*), while the finite element results underestimated the wavenumber.

As another example, we consider a linearly graded elastic layer using the state space method. In this case, the layer is divided into n uniform sublayers. The critical strain and the corresponding wave number are presented in Fig. 9 with increasing number of sublayers. It is found that the convergence of the state space solution depends on the modulus ratio, i.e., the larger the modulus ratio is, the slower the convergence rate becomes. However, even for a very large modulus ratio $(\bar{E}_0/\bar{E}_s = 1000)$, the predicted critical strain is beyond the small-strain limit for linear elasticity. The critical strain can be significantly reduced by attaching a thick, homogeneous layer (substrate) to the bottom of the linearly graded elastic layer. In this case, the plane-strain modulus varies linearly from $\bar{E}_0$ to $\bar{E}_s$ for the upper layer $(0 \le x_2 < h_f)$ and remains as a constant $\bar{E}_s$ for the underlayer $(h_f \le x_2 \le h_f + h_s)$, while

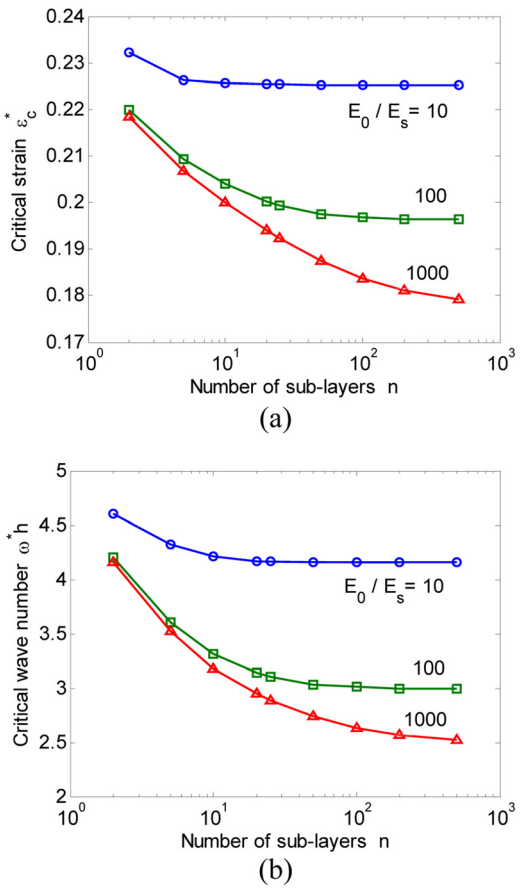

Fig. 9 Convergence of the state space solution for linearly graded elastic layers with different modulus ratios: (*a*) the critical strain and (*b*) the corresponding wave number, versus the number of sublayers used

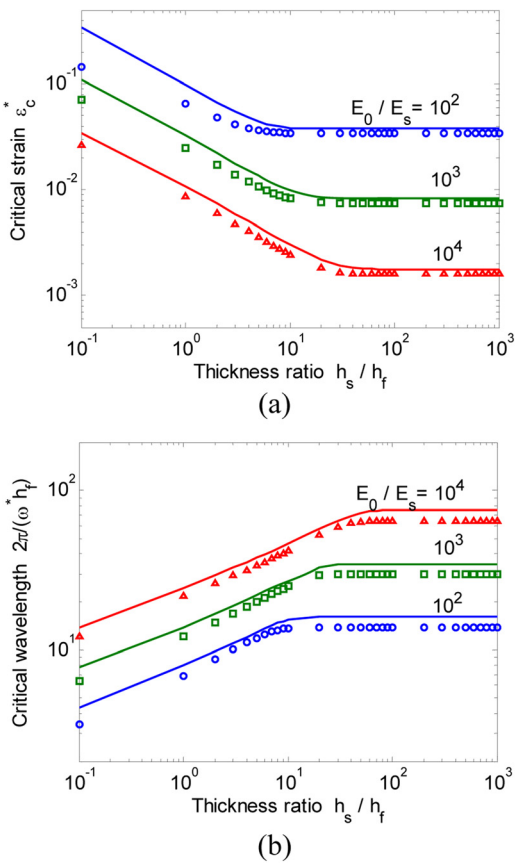

Fig. 10 (*a*) The critical strain and (*b*) the corresponding wavelength versus the thickness ratio for a linearly graded elastic layer on a homogeneous substrate. The solid lines are the analytical solution for the elastic bilayers with $\bar{E}_f = (\bar{E}_0 + \bar{E}_s)/2$ for the upper layer.

Poisson's ratio is taken to be a constant $\nu = 0.4$. To apply the state space method, the upper layer is divided into $n-1$ sublayers uniformly and the underlayer as one sublayer. For the modulus ratio $\bar{E}_0/\bar{E}_s$ ranging from 10^2 to 10^4, convergence of the state space solution is achieved by using $n \geq 50$. Figure 10 plots the critical strain and the corresponding wavelength, normalized by the upper layer thickness, for the continuously graded elastic layer. Similar to Fig. 4 for the bilayers, the critical strain and the corresponding wavelength depend on the modulus ratio ($\bar{E}_0/\bar{E}_s$) and the thickness ratio (h_s/h_f). For comparison, the analytical solution for the bilayers with the average modulus $\bar{E}_f = (\bar{E}_0 + \bar{E}_s)/2$ is shown in Fig. 10. Evidently, the bilayer approximation overestimates the critical strain and wavelength for the continuously graded elastic layers.

5 Summary

In this paper, by assuming a quadratic strain energy density function with nonlinear kinematics, we derived the governing equations for the incremental stress field in orthotropic elastic layers with the elastic properties varying in the thickness direction. Under the conditions of linear elasticity and small strain, a state space method was developed for predicting the onset of surface instability in graded elastic layers. The present method was verified by comparing to the analytical solutions for isotropic elastic bilayers and the finite element results for continuously graded elastic layers. It is found that the state space method is computationally more effective than the finite element method for multilayers with discontinuous variations in the elastic properties, while the convergence for continuously graded layers requires discretization with a sufficient number of sublayers similar to the finite element method. In addition, we note that the linear elasticity and small-strain conditions limit the present method to graded or layered materials with the critical strain less than a few percent.

Acknowledgment

RH gratefully acknowledges funding of this work by National Science Foundation through Grant No. 1200161.

Appendix: An Analytical Solution for Surface Instability of a Homogeneous Elastic Layer

Here, we present an analytical approach to solve the eigenvalue problem in Eqs. (15)–(17) for a homogeneous and isotropic elastic layer. Substituting the incremental stress components (18)–(21) into the equilibrium equations (22) and (23), we obtain

$$\mu\Delta u_{1,22} + (\lambda + 2\mu + P_{11})\Delta u_{1,11} + \lambda\Delta u_{2,21} + \mu\Delta u_{2,12} = 0 \quad \text{(A1)}$$

$$\lambda\Delta u_{1,12} + \mu\Delta u_{1,21} + (\lambda + 2\mu)\Delta u_{2,22} + (\mu + P_{11})\Delta u_{2,11} = 0 \quad \text{(A2)}$$

Inserting the perturbation displacements in Eq. (31) into Eqs. (A1) and (A2) and the boundary condition in Eq. (24), we obtain

$$\mu U_1'' - \omega^2(\lambda + 2\mu + P_{11})U_1 - \omega(\lambda + \mu)U_2' = 0 \quad \text{(A3)}$$

$$\omega(\lambda + \mu)U_1' + (\lambda + 2\mu)U_2'' - \omega^2(\mu + P_{11})U_2 = 0 \quad \text{(A4)}$$

and

$$U_1' - \omega U_2 = 0 \quad \text{and} \quad \omega\lambda U_1 + (\lambda + 2\mu)U_2' = 0, \quad \text{at} \quad x_2 = 0 \quad \text{(A5)}$$

where the single and double primes denote the first and second-order differentiations with respect to x_2. Equations (A3) and (A4) can be solved by

$$U_1(x_2) = C_1 e^{p\omega x_2} + C_2 e^{-p\omega x_2} + C_3 e^{q\omega x_2} + C_4 e^{-q\omega x_2} \quad \text{(A6)}$$

$$U_2(x_2) = -C_1 e^{p\omega x_2}/p + C_2 e^{-p\omega x_2}/p - C_3 q e^{q\omega x_2} + C_4 q e^{-q\omega x_2} \quad \text{(A7)}$$

where $p = \sqrt{1 + P_{11}/\mu}$ and $q = \sqrt{1 + P_{11}/(\lambda + 2\mu)}$. Applying the boundary conditions in Eqs. (A5) and (37), a set of algebraic equations are obtained for the coefficients C_1, C_2, C_3, and C_4, written in the matrix form as

$$\mathbf{MC} = 0 \quad \text{(A8)}$$

where $\mathbf{C} = [C_1, C_2, C_3, C_4]^T$, and

$$\mathbf{M} = \begin{bmatrix} e^{p\omega h} & e^{-p\omega h} & e^{q\omega h} & e^{-q\omega h} \\ -e^{p\omega h}/p & e^{-p\omega h}/p & -q e^{q\omega h} & q e^{-q\omega h} \\ p + 1/p & -p - 1/p & 2q & -2q \\ -2\mu & -2\mu & \lambda - (\lambda + 2\mu)q^2 & \lambda - (\lambda + 2\mu)q^2 \end{bmatrix} \quad \text{(A9)}$$

The critical condition for onset of surface instability is then predicted by setting the determinant of $\mathbf{M}$ to zero, i.e., $\det \mathbf{M} = 0$, which can be written in the same form as Eq. (43).

It is noted that the critical strain decreases with increasing wavenumber (ωh), similar to that for a hydrogel layer [22]. As a result, the minimum critical strain can be predicted by taking the wave number $\omega h \to \infty$ in Eq. (A9), with which we obtain a polynomial equation

$$\varepsilon_c^3 - 4(1 - \nu)\varepsilon_c^2 + 2(1 - \nu)(2 - \nu)\varepsilon_c - (1 - \nu)^2 = 0 \quad \text{(A10)}$$

Among the three roots to Eq. (A10), one is real-valued for $0 \leq \nu \leq 0.5$. In particular, for an incompressible elastic layer ($\nu = 0.5$), the predicted critical strain is 0.228 (compressive).

References

[1] Taber, L. A., 1995, "Biomechanics of Growth, Remodeling, and Morphogenesis," ASME Appl. Mech. Rev., **48**(8), pp. 487–545.
[2] Ohzono, T., and Shimomura, M., 2004, "Ordering of Microwrinkle Patterns by Compressive Strain," Phys. Rev. B, **69**(13), p. 132202.
[3] Guvendiren, M., Yang, S., and Burdick, J. A., 2009, "Swelling-Induced Surface Patterns in Hydrogels With Gradient Crosslinking Density," Adv. Funct. Mater., **19**(19), pp. 3038–3045.
[4] Breid, D., and Crosby, A. J., 2011, "Effect of Stress State on Wrinkle Morphology," Soft Matter, **7**(9), pp. 4490–4496.
[5] Biot, M. A., 1963, "Surface Instability of Rubber in Compression," Appl. Sci. Res. A, **12**(2), pp. 168–182.
[6] Cao, Y., and Hutchinson, J. W., 2012, "From Wrinkles to Creases in Elastomers: The Instability and Imperfection-Sensitivity of Wrinkling," Proc. R. Soc. A, **468**(2137), pp. 94–115.
[7] Allen, H. G., 1969, *Analysis and Design of Structural Sandwich Panels*, Pergamon, New York.
[8] Huang, Z. Y., Hong, W., and Suo, Z., 2005, "Nonlinear Analyses of Wrinkles in a Film Bonded to a Compliant Substrate," J. Mech. Phys. Solids, **53**(9), pp. 2101–2118.
[9] Cao, Y., and Hutchinson, J. W., 2012, "Wrinkling Phenomena in Neo-Hookean Film/Substrate Bilayers," ASME J. Appl. Mech., **79**(3), p. 031019.
[10] Gent, A. N., and Cho, I. S., 1999, "Surface Instabilities in Compressed or Bent Rubber Blocks," Rubber Chem. Technol., **72**(2), pp. 253–262.
[11] Hong, W., Zhao, X., and Suo, Z., 2009, "Formation of Creases on the Surfaces of Elastomers and Gels," Appl. Phys. Lett., **95**(11), p. 111901.
[12] Hohlfeld, E., and Mahadevan, L., 2011, "Unfolding the Sulcus," Phys. Rev. Lett., **106**(10), p. 105702.
[13] Wang Q., and Zhao X., 2014, "Phase Diagrams of Instabilities in Compressed Film-Substrate Systems," ASME J. Appl. Mech., **81**(5), p. 051004.
[14] Lee, D., Triantafyllidis, N., Barber, J. R., and Thouless, M. D., 2008, "Surface Instability of an Elastic Half Space With Material Properties Varying With Depth," J. Mech. Phys. Solids, **56**(3), pp. 858–868.
[15] Cao, Y., Jia, F., Zhao, Y., Feng, X.-Q., and Yu, S.-W., 2012, "Buckling and Post-Buckling of a Stiff Film Resting on an Elastic Graded Substrate," Int. J. Solids Struct., **49**(13), pp. 1656–1664.
[16] Diab, M., Zhang, T., Zhao, R., Gao, H., and Kim, K.-S., 2013, "Ruga Mechanics of Creasing: From Instantaneous to Setback Creases," Proc. R. Soc. A, **469**(2157), p. 20120753.

[17] Wu, Z., Bouklas, N., and Huang, R., 2013, "Swell-Induced Surface Instability of Hydrogel Layers With Material Properties Varying in Thickness Direction," Int. J. Solids Struct., **50**(3–4), pp. 578–587.
[18] Elgerd, O. L., 1967, *Control System Theory*, McGraw-Hill, Kogakusha, Inc., Tokyo.
[19] Derusso, P. M., Roy, R. J., Close, C. M., and Desrochers, A. A., 1998, *State Variables for Engineers*, John Wiley & Sons, Inc., New York.
[20] Fan, J., and Ye, J., 1990, "An Exact Solution for the Statics and Dynamics of Laminated Thick Plates With Orthotropic Layers," Int. J. Solids Struct., **26**(5–6), pp. 655–662.
[21] Jia, F., Cao, Y., Zhao, Y., and Feng, X.-Q., 2014, "Buckling and Surface Wrinkling of an Elastic Graded Cylinder With Elastic Modulus Arbitrarily Varying Along Radial Direction," Int. J. Appl. Mech., **6**(1), p. 1450003.
[22] Kang, M. K., and Huang, R., 2010, "Swell-Induced Surface Instability of Confined Hydrogel Layers on Substrates," J. Mech. Phys. Solids, **58**(10), pp. 1582–1598.
[23] Chen, X., and Hutchinson, J. W., 2004, "Herringbone Buckling Patterns of Compressed Thin Films on Compliant Substrates," ASME J. Appl. Mech., **71**(5), pp. 597–603.
[24] Huang, R., 2005, "Kinetic Wrinkling of an Elastic Film on a Viscoelastic Substrate," J. Mech. Phys. Solids, **53**(1), pp. 63–89.
[25] Cai, S., Breid, D., Crosby, A. J., Suo, Z., and Hutchinson, J. W., 2011, "Periodic Patterns and Energy States of Buckled Films on Compliant Substrates," J. Mech. Phys. Solids, **59**(5), pp. 1094–1114.